Exp Fluids (2007) 42:441–457
DOI 10.1007/s00348-007-0252-z

RESEARCH ARTICLE

Near wall characterization of the flow over a two-dimensional steep smooth hill

J. B. R. Loureiro · F. T. Pinho · A. P. Silva Freire

Received: 28 December 2005 / Revised: 22 December 2006 / Accepted: 22 January 2007 / Published online: 7 February 2007

Abstract Near-wall data for the strongly perturbed flow in a neutrally stable boundary layer encountering a steep, smooth, two-dimensional hill are presented. Observations were made on the centerplane of a water channel at thirteen stations relative to the hill by laser Doppler anemometry. The large reverse flow region that is formed on the lee of the hill was particularly scrutinized through seven measuring stations. Results are presented for the mean and turbulent properties of the flow. Wall shear stress was evaluated through fitting procedures that resorted to the near wall behavior of the velocity profile. Logarithmic fits as well as predictions through the Reynolds stress profiles are also presented.

Keywords Near wall turbulence · Steep hill · Wall shear stress

1 Introduction

Boundary layers developing over surfaces that present a change in elevation are a common occurrence in nature and in technology. In fact, the large number of works that can be found in literature devoted to this subject are a clear tribute to its relevance. In the early studies, emphasis was placed on the experimental characterization of the flow (e.g. Mason and Sykes 1979; Arya et al. 1987), and on the construction of asymptotic theories (e.g. Jackson and Hunt 1975; Hunt et al. 1988). Recently, investigations have preferred the use of non-linear numerical models (e.g. Castro and Apsley 1997; Hewer 1998; Allen and Brown 2002).

In this work, the original trend will be exercised once again. In particular, the paper will discuss flows over a two-dimensional, steep, smooth hill from an experimental point of view. Special attention will be placed on the characterization of the region of reverse flow.

In the variety of applications concerning flows over wall elevations two fields stand out: aeronautics and meteorology. In the former, wall elevations are normally referred to as bumps and the flow is observed to develop over a smooth wall. In the latter, the changes in topography are called hills and the flow develops over a rough surface. Despite the intrinsic differences in the wall boundary condition, both fields share a common limitation: the complete understanding of the mechanisms that govern flow separation.

For flows over a smooth surface, and provided separation is present, any appropriate near wall flow scaling will depend basically on the following parameters: viscosity, local wall shear stress and local wall pressure gradient. In fact, flows subject to large pressure-gradients are observed to experience a large wake velocity deficit. Under this condition, the classical matching arguments of the asymptotic theory of Millikan (1939) break down, implying that the canon-

J. B. R. Loureiro (✉) · A. P. Silva Freire
Mechanical Engineering Program (PEM/COPPE/UFRJ),
C.P. 68503, 21945-970 Rio de Janeiro, Brazil
e-mail: jbrloureiro@mecanica.coppe.ufrj.br

F. T. Pinho
Centro de Estudos de Fenómenos de Transporte,
Faculdade de Engenharia da Universidade do Porto,
Rua Dr. Roberto Frias s/n, 4200-465 Porto, Portugal

F. T. Pinho
Universidade do Minho, Largo do Paço,
4704-553 Braga, Portugal

ical two-layered asymptotic structure of the boundary layer does not hold anymore. In particular, close to a separation point, the friction velocity $u_*(=\sqrt{\tau_w/\rho})$ tends to zero and becomes an inappropriate scaling parameter. This forces into the problem a new scaling parameter based on the local pressure gradient, u_{pv} $(=((\nu/\rho)(\partial p/\partial x))^{1/3})$, that is used to accommodate a new multi-layered structure (Sychev and Sychev 1980; Durbin and Belcher 1992). This new scaling velocity was first introduced by Stratford (1959), who showed that a power-law velocity profile exists at a separation point. In further studies, several authors have attempted to embed the classical two-layered structure and Stratford's local solution into a single theoretical framework. Typical examples are the works of Mellor (1966), of Afzal (1983), of Nakayama and Koyama (1984), of Melnik (1989) and of Cruz and Silva Freire (1998, 2002). These authors have basically used asymptotic arguments to construct different scaling laws that reduce to the relevant laws at the appropriate limiting cases. These formulations clearly need to be tested against reliable experimental data.

For flows over a rough hill, the relevant scaling parameters are quite different. The roughness elements completely remove the viscous layer, yielding a very complex flow pattern whose properties must now be scaled against characteristic lengths dictated by the roughness itself. In situations where just a small perturbation to the velocity field occurs so that the flow remains attached, the equations of motion can be linearized to yield a flow structure consisting of two-layers (Jackson and Hunt 1975; Hunt et al. 1988). The linear theory produces expressions for the relevant scaling parameters and for the speedup. Unfortunately, in situations where perturbations are large enough so that flow separation occurs, no theory of rough wall separation similar to those described in the previous paragraph can be found. In fact, the sensitivity of flow separation to wall roughness is known to be marked even on steep hills.Quantifying the onset and extent of separation, however, on flows over a rough wall and subject to strong adverse pressure-gradients has proved to be a very challenging problem.

The above remarks give cause to the following statement: comprehensive asymptotic theories that have been proposed to describe the flow near a separation point need to be tested against reliable near wall measurements. At this stage, to work with flows over a smooth hill can give us access to a valuable validation parameter: the wall shear stress. This quantity is of essential importance to the understanding of turbulent flow and to the validation of theoretical and numerical procedures, but is also very difficult to evaluate for flows over curved and rough surfaces. Over a smooth surface, however, provided detailed experimental data are obtained, the wall shear stress distribution can be estimated from mean velocity fits across the viscous sublayer and the turbulent logarithmic region. In particular, results for the entire region of reverse flow can be obtained.

As a further motivation, we point out that turbulent flows over steep, smooth hills are a particularly difficult test to turbulence models. Wang et al. (2004) have specifically raised this point, adding that much of the effort concerning the investigation of turbulence closures does not tackle separation provoked by smoothly varying adverse pressure gradients. In particular, these authors argue that numerical simulations of flows over two-dimensional hills show that many turbulence models overestimate the size of the recirculation region, and that this fact may be associated with an insufficient level of shear stress in the separated shear layer. For computations over three-dimensional hills, none of the present models are observed to perform well.

Therefore, the numerical simulation of the flow over a steep hill is a problem that typically demands detailed experimental validation. In particular, a usual difficult problem faced by turbulence models is the correct prediction of the large gradients in flow variables in the near wall region. The hill summit and the region of reversed flow are also very challenging in terms of numerical prediction as previously reported in the literature (see, e.g. Ying and Canuto 1997; Iizuka and Kondo 2004). Unfortunately, near wall data sets for the separated flow region on the lee of a hill are not widely available in literature. For example, the works of Ishihara et al. (2001) and Ross et al. (2004) present comprehensive experimental studies on the flow over steep hills. However, in none of these works, the near wall region is well characterized.

The main purpose of this work is hence to carry out a single and detailed experiment to redeem the lack of near wall data for separated flow over a smooth hill. Thus, measurements must be detailed enough to characterize the near wall viscous region. The experiments were conducted in a water channel and considered a two-dimensional hill, steep enough to provoke a large separated flow region on its lee side. Flow properties were characterized by laser Doppler anemometry at 13 stations, 7 of which are in the reverse flow region. Near wall resolution was enough to consider at least eight points in the first 3 mm away from the wall. Results include complete profiles of the mean velocity components u and w, two-dimensional Reynolds stress tensor elements $\overline{u'u'}, \overline{w'w'}$ and $-\overline{u'w'}$,

mixing-length L and eddy-viscosity ν_t distributions, wall shear stress distribution and turbulence production. The overall implication is that these data form a comprehensive set against which numerical computations of near wall flow over a hill can be tested.

The wall shear stress is a parameter of very difficult experimental assessment. An outline of the techniques available for the measurement of skin-friction in turbulent boundary layer is given in Winter (1977). In early studies, the characterization of the instantaneous or mean reverse flow and of the wall shear stress near incipient separation was almost an impossible task due to the lack of appropriate instrumentation. With the development of the pulsed-wire and of the laser-Doppler anemometer, some reliable experimental data of this quantity could be obtained (e.g. Simpson et al. 1981; Thompson and Whitelaw 1985; Dengel and Fernholz 1990). A discussion about wall shear stress determination through polynomial fits has been introduced by Durst et al. (1996). These authors have used laser-Doppler anemometry and direct numerical simulation data, but the analysis was restricted to attached flows. Naqwi and Reynolds (1987) show that optical methods based on laser-Doppler anemometry that rely on linearly varied fringe spacing are able to directly measure the shear stress provided there is no slip at the wall.

Here, wall shear stress distribution was obtained from mean velocity profiles through fits to the viscous sublayer and to the turbulent logarithmic region. In addition, and where conditions permitted, the wall shear stress was also obtained by extrapolation to the wall of the shear stress profiles. The present work is very strict about the determination of the wall shear stress because, for separated flow over a hill, the number of available data sets is small. Results based on chart methods are normally shown in literature without their statistics. We discuss the calculations showing fitted profiles in log-linear coordinates and the entire statistics of the fitting process. In view of the detailed procedure that was used to find the wall shear stress distribution, we consider the present data to be reference data.

2 Experimental apparatus

2.1 Description of water-channel and instrumentation

The experiments were carried out in one of the open-channels of the Hydraulics Laboratory of the Civil Engineering Department, University of Oporto, Portugal. The water channel is 17 m long with a cross section of 40 cm width per 60 cm height. The water recirculation system consists of two underground tanks, four pumps with a maximum capacity of 150 l s^{-1} and one upper stabilizing tank. The working section has glass side walls and is 3 m in length. The model hill top was located 8 m from the channel entrance. An illustration of the test section is given in Fig. 1.

In a typical experimental run, two pumps sufficed to keep the system running in a steady state, with a maximum flow rate variation of ±0.8%. At the entrance of the channel, flow stabilization and uniformization was achieved with the use of a series of screens and filters in order to suppress any excessive level of turbulence. To guarantee an accurate flow rate control, a magnetic flowmeter was installed in the supply line. The water depth along the channel was controlled by a vertical steel gate.

A one component, fiber optic, Dantec laser-Doppler anemometry system was used in the forward scatter mode to measure the mean and the fluctuating velocity fields. The laser was a 2 W Ar-ion source operating in multi-mode. A Bragg cell unit was used to introduce an electronic shift of 0.6 MHz to resolve flow direction. Front lenses with 310 mm focal length were mounted on the probe in order to accurately position the measurement volume on the centerline of the channel. Before being collected by the photomultiplier, the scattered light passed through an interference filter of 514.5 nm, so that only green light was acquired. The signal from the photomultiplier was band-pass filtered and processed by a TSI 1990C counter, operating in single measurement per burst mode. A series of LDA biases were avoided by adjusting the strictest parameters on the data processor. For each point measured, a sample size of 10,000 values has been considered. This

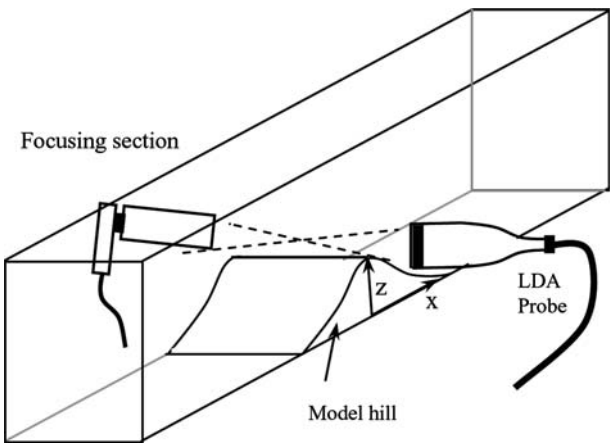

Fig. 1 Illustration of the test section, the model hill and the LDA system

sample size was observed to be sufficient to assure independent velocity results at each point measured. Table 1 lists the main characteristics of the laser-Doppler system used.

The above procedure was used to measure both the horizontal and the vertical velocity components. To obtain the Reynolds shear stresses, measurements were made by turning the probe to the positions ±45° according to the procedure described by Logan (1972). For the undisturbed flow region, the uncertainties in the mean velocity components u and w are lower than 0.2% of the free stream velocity, u_δ. Downstream of the hilltop, in high level turbulence regions, these uncertainties increase to about 0.3% of the free stream velocity. For the fluctuating quantities, $\sqrt{\overline{u'^2}}$, $\sqrt{\overline{w'^2}}$, and $-\overline{u'w'}$, the estimated uncertainties in the undisturbed flow region are of 2.3, 1.8, 4.2% of the friction velocity in the undisturbed flow (for the Reynolds shear stress the uncertainty is given in percentage of the square of the friction velocity of the undisturbed flow), respectively, increasing to 3.8, 3.5 and 6.9% in regions of high turbulence. The LDA traversing system was 3D and had a positioning precision of ±10 μm.

2.2 Model hill characteristics

The model hill used in the present work was two-dimensional and aerodynamically smooth. Following other authors, see e.g. Britter et al. (1981) and Arya et al. (1987), the profile shape of the hill was that of a modified "Witch of Agnesi" profile, given by

$$z_H(x) = H_1[1 + (x/L_H)^2]^{-1} - H_2. \quad (1)$$

Thus, H (= H_1–H_2)(=60 mm) is the hill height and L_H (=150 mm) is the characteristic length of the hill representing the distance from the crest to the half-height point. Co-ordinates, x and z represent the horizontal and vertical axes, respectively, as shown in Fig. 2.

The geometry of the model was chosen so as to simulate a steep hill with a large recirculation region. The model was made of a single sheet of polished acrylic. The characteristic parameters of the hill are presented in Table 2.

Table 1 Main characteristics of the laser-Doppler system

Wavelength	514.5 nm
Half-angle between beams	3.415°
Fringe spacing	4.3183 μm
Frequency shift	0.60 MHz
Dimensions of the measurement volume	
Major axis	1.53 mm
Minor axis	162.0 μm

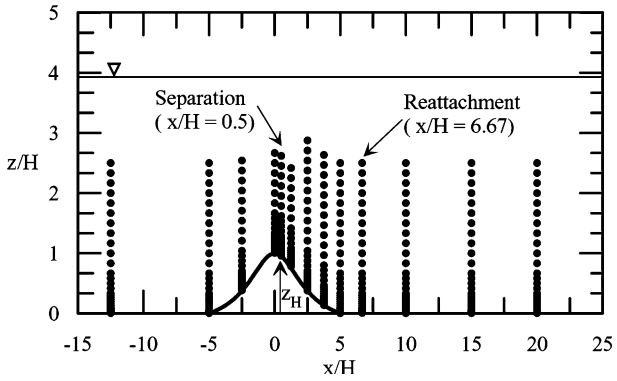

Fig. 2 Position of measuring stations and co-ordinate system

3 Results: mean velocity and Reynolds stresses

Measurements were made on the channel centerplane at the 13 stations illustrated in Fig. 2. Please note the position of the rectangular Cartesian coordinate system.

3.1 Boundary layer flow in the absence of the hill

Measurements of mean and turbulent velocities have been performed along the working section in the absence of the hill. The results show that the boundary layer is in a fully developed state at the time the working section is reached.

Figure 3a compares the horizontal mean velocity profile measured in the absence of the hill (at station $x/H = 0$) with the velocity profile measured upstream of the hill at station $x/H = -12.5$. Lengths and velocities were normalized, respectively, with the boundary layer thickness, δ, and the free-stream velocity, u_δ. The vertical mean velocity profiles in both stations assumed a nearly constant value of 0.008 u_δ. Figure 3b illustrates the behavior of the longitudinal Reynolds stresses at the same stations.

These results show that the profiles at station $x/H = -12.5$ are not influenced by the presence of the hill so that no significant flow blockage effects are present. On this ground, profiles taken at station $x/H = -12.5$ can be

Table 2 Hill features

Characteristic height	H_1	75 mm
Characteristic height	H_2	15 mm
Hill height	H	60 mm
Hill length	L	600 mm
Distance from the crest to the half-height point	L_H	150 mm
Aspect ratio	$L/2(H)^{-1}$	5
Maximum slope	θ_{max}	18.6°

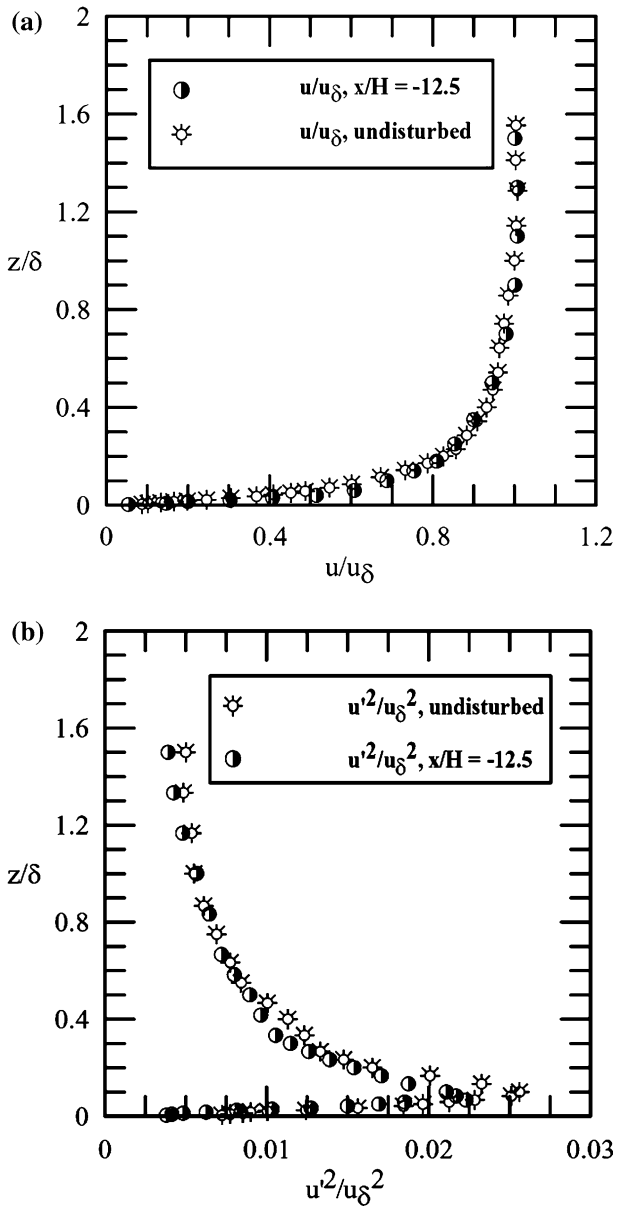

Fig. 3 Velocity and turbulence profiles at $x/H = -12.5$ compared with those measured in the absence of the hill ($x/H = 0.0$). **a** Longitudinal and vertical mean velocity profiles. **b** Longitudinal Reynolds stress profiles

Table 3 Properties of undisturbed profile ($x/H = -12.5$)

Boundary layer thickness	δ	100 mm
External velocity	u_δ	0.0482 m s^{-1}
Reynolds number	R_δ	4,772
Friction velocity	u_*	0.0028 m s^{-1}
Roughness length	z_0	0.27 mm
Longitudinal velocity fluctuations at (z/δ=0.05)	$\sqrt{\overline{u'^2}}/u_*$	2.50
Transversal velocity fluctuations at (z/δ=0.08)	$\sqrt{\overline{w'^2}}/u_*$	0.83

considered a good approximation to the undisturbed boundary layer profiles.

The local properties of the boundary layer in the undisturbed flow are shown in Table 3. To put the present work into perspective, these values are compared with other typical values of near surface turbulence in neutrally stratified flows: $\sqrt{\overline{u'^2}}/u_* = 2.3$ and $\sqrt{\overline{w'^2}}/u_* = 1.1$ (Grant 1992), $\sqrt{\overline{u'^2}}/u_* = 2.12$ (Britter et al. 1981), $\sqrt{\overline{u'^2}}/u_* = 2.5$ and $\sqrt{\overline{w'^2}}/u_* = 1.2$ (Khurshudyan et al. 1981), $\sqrt{\overline{u'^2}}/u_* = 2.2$ and $\sqrt{\overline{w'^2}}/u_* = 1.0$ (Gong and Ibbetson 1986) and $\sqrt{\overline{u'^2}}/u_* = 2.19$ and $\sqrt{\overline{w'^2}}/u_* = 1.12$ (Athanassiadou and Castro 2001).

To evaluate the two-dimensionality of the flow, mean velocity measurements were obtained in x–z planes (see Fig. 2) located 5 cm to either side of the channel centerplane. When the hill was not in place, the results showed a variation of 2% in relation to measurements taken at the channel centerplane. In the presence of the hill, such differences in velocity measurements were of about 3%.

3.2 Flow behavior over the hill

Presentation of the data will be divided into three parts: data for the flow field upstream of the separation point (first 3 stations), data for the separated flow region (next 7 stations) and data for the returning to equilibrium region (last 3 stations). Following the procedure of previous authors, the hill height H and the undisturbed external boundary layer mean velocity u_δ will be used as reference parameters. A dash will denote turbulent quantities.

The mean horizontal and vertical velocity profiles are shown in Figs. 5 and 6, respectively, where solid lines were used to connect identical symbols to improve legibility. The region of accelerated flow on the upstream side of the hill is illustrated in Fig. 5a. At the crest of the hill, the streamwise velocity profile becomes nearly uniform.

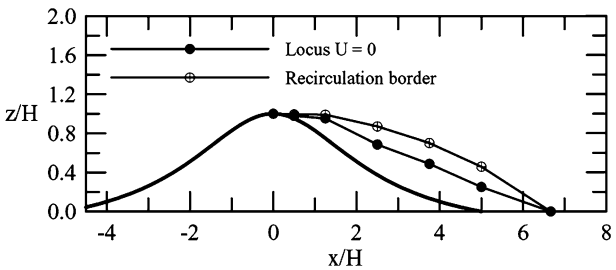

Fig. 4 Locus of zero longitudinal velocity and outline of region of trapped flow inside the re-circulation region

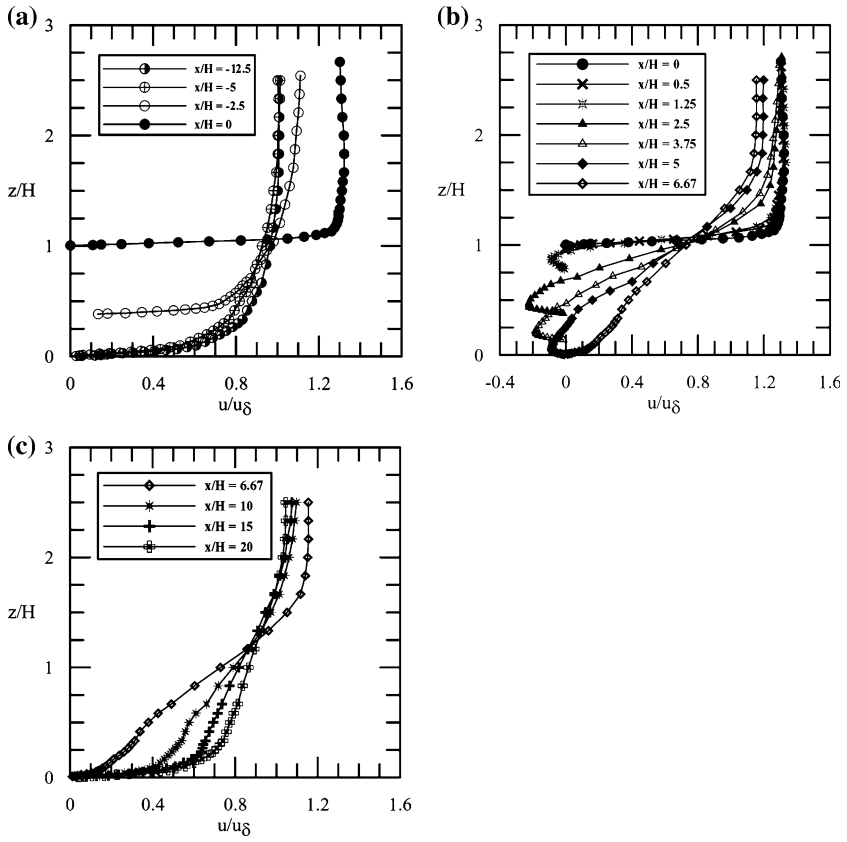

Fig. 5 Longitudinal mean velocity profiles: **a** upstream of the separation, **b** separation region, **c** downstream of the reattachment point

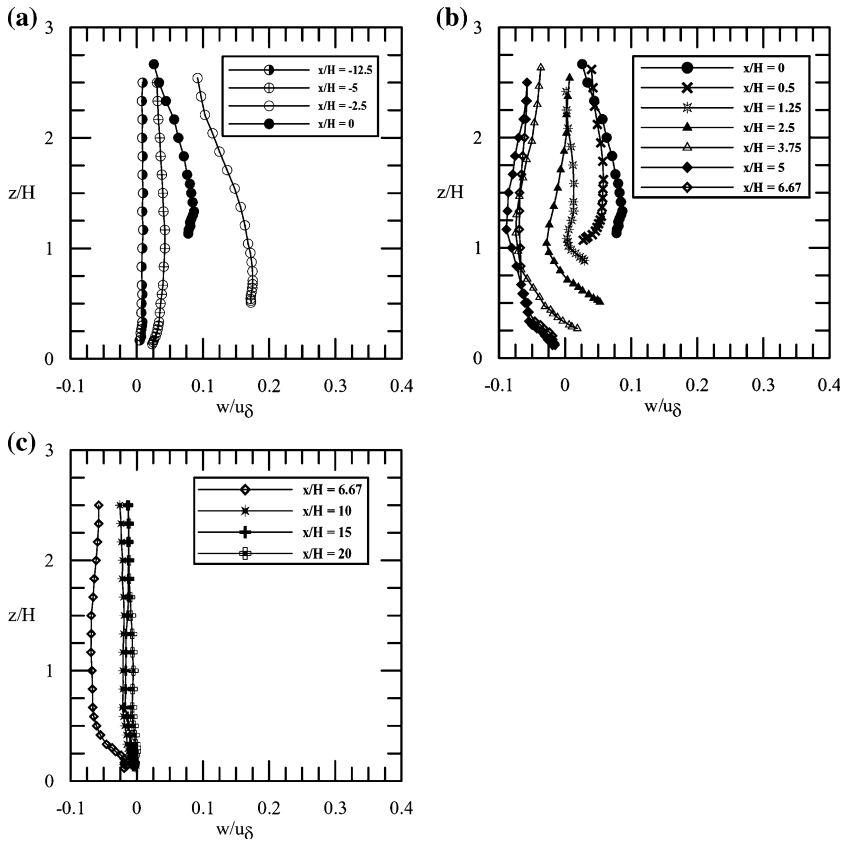

Fig. 6 Vertical mean velocity profiles: **a** upstream of the separation, **b** separation region, **c** downstream of the reattachment point

Figure 4 shows the extent of separated flow, as characterized by the curve defined by the points where the mean streamwise velocity is zero. An estimation of the region of trapped recirculating flow is also shown. The flow separates at $x/H = 0.5$ and reattaches at about $x/H = 6.67$. This results in a bubble length of about $x/H = 6.17$.

The separated flow region is shown in Fig. 5b. Figure 5c shows the four velocity profiles measured downstream of the separated flow region. Profiles at $x/H = 10$ and 15 present a large momentum-deficit in comparison to the undisturbed profile; even at $x/H = 20$ the boundary layer has not yet fully recovered from separation effects.

The large-increase in the vertical mean velocity profile, w, on the upstream side of the hill is shown in Fig. 6a. At station $x/H = -2.5$, as the streamlines follow the upwind slope of the hill, w increases as much as seventeen times when compared to values at $x/H = -12.5$. The velocity profiles on the downside of the hill are shown in Fig. 6b. From stations $x/H = 0$ to $x/H = 2.5$, the flow vertical velocity is still positive due to the separation bubble that is formed. Past station $x/H = 2.5$, negative values of w are observed. As the flow approaches station $x/H = 10$ (Fig. 6c), w returns to a near zero value.

The changes in Reynolds stresses are shown in log-linear coordinates in Figs. 7, 8 and 9; solid lines are used to connect identical symbols. In the accelerated flow region upstream of the hill (Fig. 7a), $\overline{u'^2}$ is observed to decrease slightly along the upwind slope ($x/H = -2.5$), until the crest is reached. At the hill top, $\overline{u'^2}$ about recovers its undisturbed peak value, but a small difference as compared to station $x/H = -12.5$ is noted above the peak height.

In the separated flow region (Fig. 7b), $\overline{u'^2}$ increases by a factor of five. In addition, the large increase in peak values for $\overline{u'^2}$, as well as its increasing distancing from the wall toward the shear layer results from the turbulence production term $P_{uu} = -2\overline{u'w'}(\partial u/\partial z)$. The maximum peak value for $\overline{u'^2}$ is located at coordinates $x/H = 3.75$, near the center of the recirculation bubble, and $z/H = 0.8$, approximately at the shear layer that bounds the recirculation bubble. In general, in this region, turbulence profiles are characterized by an elevated maximum, whose distance to the wall increases with increasing distance from the hill. Downstream of the hill (Fig. 7c), at stations $x/H = 15$ and 20, the $\overline{u'^2}$ profiles can still be distinguished from each other and from the undisturbed profile.

The behavior of $\overline{w'^2}$ on the hill top is slightly different from the behavior of $\overline{u'^2}$, for $\overline{w'^2}$ suffers a relative

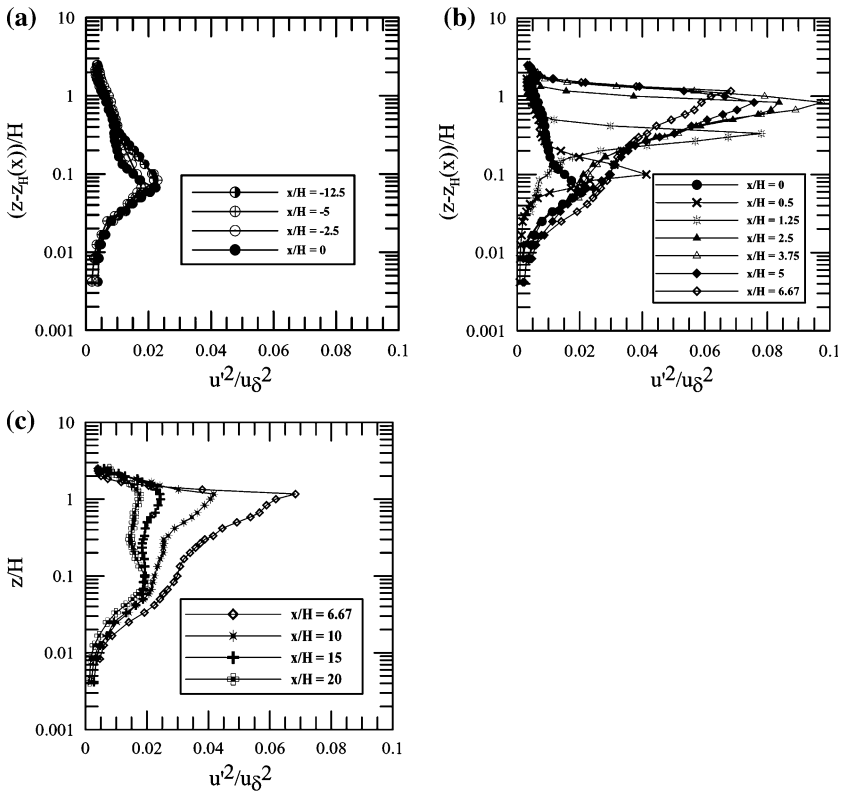

Fig. 7 Normalized streamwise Reynolds stress profiles, u'^2/u_δ^2: **a** upstream of the separation, **b** separation region, **c** downstream of the reattachment point

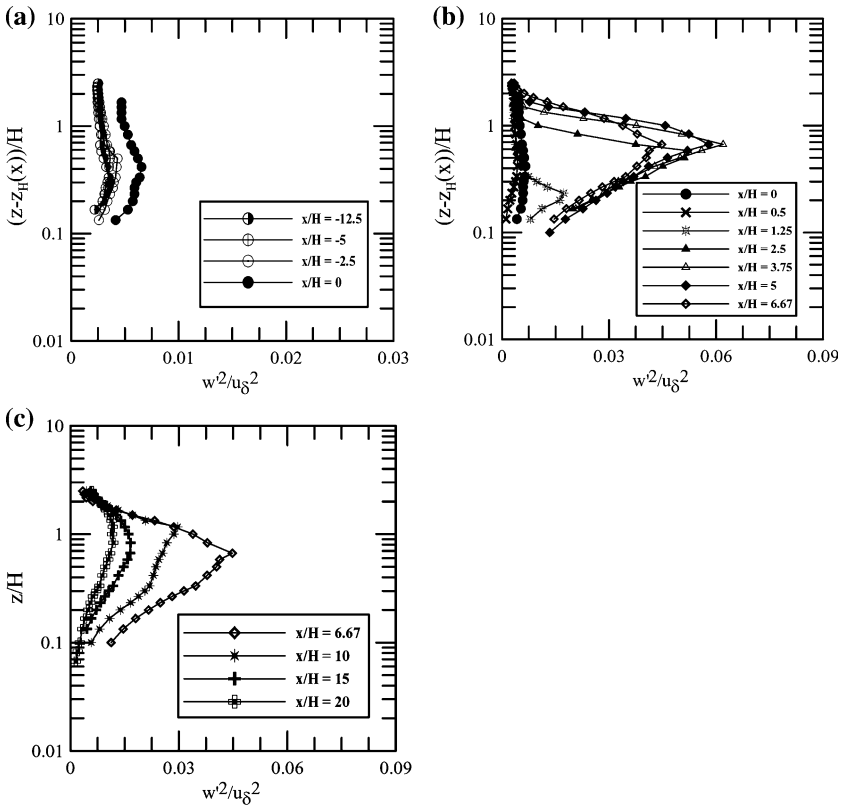

Fig. 8 Normalized vertical Reynolds stress profiles, w'^2/u_δ^2: **a** upstream of the separation, **b** separation region, **c** downstream of the reattachment point

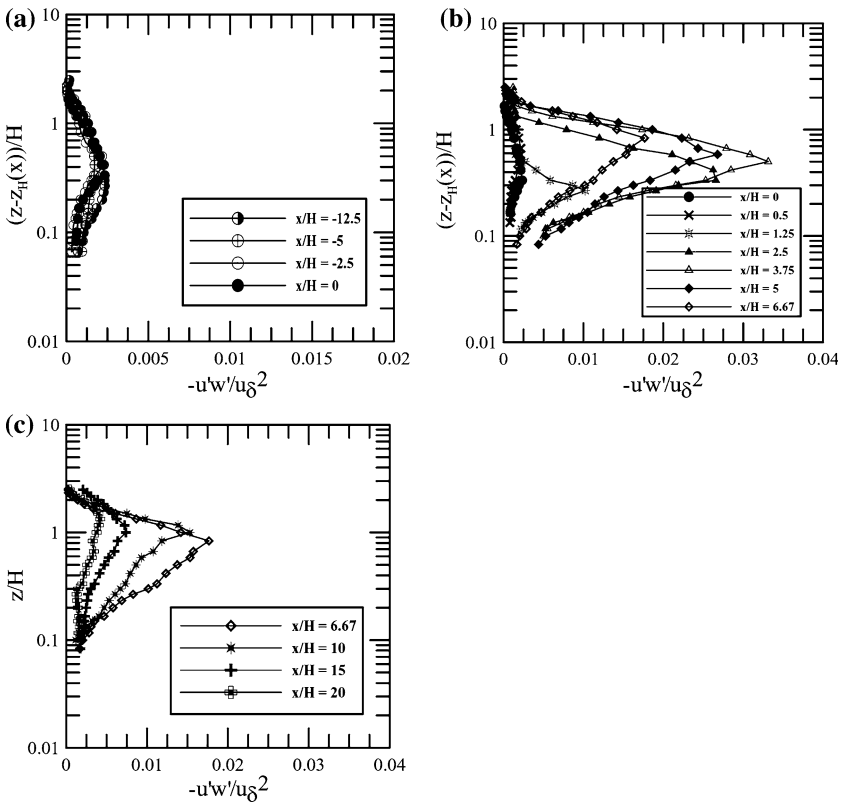

Fig. 9 Normalized Reynolds shear stress profiles, $-\overline{u'w'}/u_\delta^2$: **a** upstream of the separation, **b** separation region, **c** downstream of the reattachment point

increase of about 80% as compared to the undisturbed values (Fig. 8a). This increase is followed by a further, and a much stronger increase, of about 20-fold in the separated flow region (Fig. 8b). Indeed, we had seen previously that a large increase in w was observed uphill. The role of this increase is, in its turn, to increase the production of $\overline{w'^2}$ through $P_{ww} = -2\overline{u'w'}(\partial w/\partial x)$.

The distributions of $\overline{u'^2}$ and $\overline{w'^2}$ are somewhat similar across the separated region, but for the fact that $\overline{w'^2}$ is about 65% smaller than $\overline{u'^2}$. This is due to the turbulence production term $P_{uu} = -2\overline{u'w'}(\partial u/\partial z)$, that is expected to exceed $P_{ww} = -2\overline{u'w'}(\partial w/\partial x)$, since in this region $(\partial u/\partial z) > (\partial w/\partial x)$. Also, we note that the maximum value of $\overline{w'^2}$ is found at $x/H = 3.75$, $z/H = 0.8$, just as we have quoted for $\overline{u'^2}$. Far away from the hill, at stations $x/H = 15$ and 20, the two $\overline{w'^2}$ profiles are still very different from each other (Fig. 8c).

Regarding the Reynolds shear stress, on the upwind side of the hill the profiles are not too different and stresses are low but increase slowly with height (Fig. 9a). Notable changes in $-\overline{u'w'}$ are observed just as the flow passes station $x/H = 1.25$. Then, a large increase in $-\overline{u'w'}$ is observed, of the order of seventeen times. This behavior can be explained by the enhanced shear effects through the production term $P_{u'w'} = 2\overline{w'^2}(\partial u/\partial z)$. Differently from the peak locations for $\overline{u'^2}$ and $\overline{w'^2}$, the highest peak value of $-\overline{u'w'}$ is found at position $x/H = 3.75$, $z/H = 0.6$. No inner region of constant $-\overline{u'w'}$ was found in the separated flow region (Fig. 9b). Downstream of the hill, at stations $x/H = 15$ and 20, $-\overline{u'w'}$ shows a nearly constant value in the inner region, but the difference in the values of $-\overline{u'w'}$ between these stations is almost by a factor of two (Fig. 9c).

4 Wall shear stress

Most of the methods used to measure the wall shear stress rely in one way or another on the hypothesis that in the boundary layer, the mean velocity profile assumes a logarithmic form at a certain distance from the wall. In fact, chart methods based on the existence of a logarithmic velocity profile have become so popular that some classifications of the available techniques frequently separate them into techniques that comply to the conditions set by the classical law of the wall and those that do not. The Preston tube and the Clauser-chart method are, of course, strongly dependent on the log-law assumption.

In a separation region, the near wall flow will not follow a logarithmic profile. Thus, other techniques should be used to measure the wall shear stress: direct methods, analogies or liquid tracers. In our problem, the curved surface prevents the use of balances or the pulsed heated film technique. Thus, for the type of flow to be studied here, the only feasible way to find the wall shear stress is through a detailed analysis of the velocity profiles in the viscous wall region. In addition, for stations outside of the separation bubble, the wall shear stress will be evaluated by three methods: (1) through the slope of the velocity profile in the viscous sublayer, (2) through the classical logarithmic velocity profile and (3) by considering the existence of a region adjacent to the wall in which the total shear stress is nearly constant.

In a turbulent boundary layer, the very near wall region is dominated by viscous effects. Under pressure gradient conditions, the viscous sub-layer equation can be written in rectangular Cartesian coordinates as

$$\mu\frac{\partial^2 u}{\partial z^2} = \frac{\partial P}{\partial x}, \tag{2}$$

where u stands for the streamwise mean velocity and P for mean pressure.

A double integration of the above equation furnishes

$$u = \frac{1}{2\mu}\frac{\partial P}{\partial x}z^2 + \frac{\rho u_*^2}{\mu}z, \tag{3}$$

with $u_* = \sqrt{\tau_w/\rho}$.

Equation 3 can be re-cast in a non-dimensional format as

$$\frac{u}{u_*} = \left(\frac{\nu}{2\rho}\frac{1}{u_*^3}\frac{\partial P}{\partial x}\right)\left(\frac{zu_*}{\nu}\right)^2 + \frac{zu_*}{\nu}, \tag{4}$$

or else

$$u^+ = p^+ z^{+2} + z^+, \tag{5}$$

a form that is commonly found in literature.

Thus, provided detailed measurements are made in the viscous region, Eq. 3 can be used to find not only u_* but also $\partial P/\partial x$. In principle, Eq. 3 should be valid in the whole flow region giving us a method to find u_* even in the flow separated region.

In the attached flow region, in places where the logarithmic velocity profile can be discriminated and pressure-gradients are negligible, the classical law of the wall equation reads

$$\frac{u}{u_*} = \frac{1}{\varkappa}\ln\frac{zu_*}{\nu} + A, \tag{6}$$

where $\varkappa = 0.4$ and $A = 5.0$. According to Eq. 6, a plot of u against $\ln(z)$ provides the friction velocity through the slope $u_*/\varkappa$.

In a third procedure, consider the turbulent shear stress, $-\rho\overline{u'w'}$, to be the dominant part of the total shear stress outside the viscous layer. Then introducing Prandtl's (1925) assumption that in the neighborhood of the wall the shear stress remains constant, we have

$$-\overline{u'w'} = {u_*}^2. \tag{7}$$

To estimate the friction velocity from Eqs. 3 and 6, we must then consider the problem of fitting sets of data points in the viscous and logarithmic regions of the boundary layer. The best curve fits are found by inspection of the coefficient of determination, R-squared (R_{sq}), defined by

$$R_{sq} = \frac{\Sigma_r}{\Sigma_e + \Sigma_r} \tag{8}$$

where Σ_e is the residual sum of squares (sum of the squares of all the residual values) and Σ_r is the regression sum of squares (sum of squares of the differences between the average of all u values and the fit u values at each z location where a data point occurs).

The sets of points to be included in the analysis were initially determined by considering the expected range of validity of the local solutions. Next, the lower and upper bounds of the fits were varied arbitrarily until the best curve was found by searching for the highest value of R_{sq}. The coefficient of determination, R-squared shows how well the data are explained by the best-fit line (Bevington 1969).

For flows over a flat wall, the x-coordinate can be aligned with the mean flow direction, resulting in a rectangular Cartesian system, where the momentum balance in x-direction contains most of the relevant dynamical information. In this coordinate system, experimental points are easily located and derivatives evaluated so that Eqs. 3, 6 and 7 can be used directly to evaluate u_* from given values of u and of $-\overline{u'w'}$ as a function of z.

For flows over curved surfaces, however, identifying a coordinate system where the main coordinate axis is aligned with the flow direction is a problem. Close to the wall, the main coordinate axis can be aligned with the tangent to the surface, resulting in a surface-oriented coordinate system s–n. Considering that close to the surface the flow velocity must remain parallel to the wall, system s–n can be used to find local properties of the flow. The problem is that far away from the wall, the flow velocity will be approximately horizontal resulting in a mismatch between the chosen s–n coordinate system and the flow parameter to be measured. To overcome this difficulty, Finnigan (1983) suggests the use of physical streamlined coordinates which avoid the practical problem of aligning instruments in a surface-oriented coordinate frame, a tricky practical problem. This alternative coordinate system is, however, difficult to use in separated flow regions. Thus, most of the data presented in literature for flows over hills follow a rectangular Cartesian system.

In our worst case scenario, the wall tangent corresponds to an angle, α, of about 14° (station $x/H = 1.25$). Since $\sin\alpha = 0.24$, the corresponding streamwise velocity displacement along the normal direction will occur over a maximum distance of $\Delta s = 0.7$ mm. This fact, allied to the fact that $u > > w$, means that close to the wall the friction velocity can be calculated directly from Eqs. 3, 6 and 7 with the rectangular Cartesian system shown in Sect. 3.

One major concern in using laser-Doppler anemometry data to estimate wall shear stress from slopes of the mean velocity profiles is the uncertainty in determining the absolute distance from the wall. This is an inherent difficulty of this technique, related to the finite size of the measurement volume. Following a procedure described in Durst et al. (1996), we have determined the wall location to within 64 μm ($z^+ = 0.18$), a distance that corresponds to 40% of the measurement volume.

Uncertainties in the evaluation of u_* must then be assessed according to uncertainties resulting from wall curvature and wall location effects. This will be made considering regions of low and high turbulent motions. Over the flat wall, in regions of low turbulence, the uncertainties in u_* are 1.05, 0.43 and 2.6% for estimations obtained through the viscous, logarithmic and shear stress profiles, respectively. In regions of high turbulence, these uncertainties change to 2.8, 0.44 and 1.4%, respectively. Over the curved wall, uncertainties are 1.05% (viscous region), 1.46% (log-profile) and 2.8% (shear stress profile) for regions of low turbulence and 2.8% (viscous region), 1.03% (log-profile) and 1.5% (shear stress profile) for regions of high turbulence.

4.1 Viscous region analysis

Mean velocity profiles in the viscous sublayer upstream of the hill top were characterized by seven experimental points in the range $0.5 \leq z^+ \leq 6$. For each station, the local velocity profile was fitted to a straight-line according to Eq. 3. Indeed, note that as $\partial P/\partial x \rightarrow 0$, the second degree polynomial fit provided by Eq. 3

reduces to a linear fit through the origin. Thus, only in regions where $\partial P/\partial x$ is significant the full equation has to be retained.

From the hill top to the end of the reverse flow region, mean velocity profiles are shown in Fig. 10a in linear coordinates. The near wall behavior for these stations is shown in detail in Fig. 10b. All considered stations, with the exception of station $x/H = 1.25$, had at least eight points located within the first 3 mm ($0.2 \leq z^+ \leq 5.0$) of the viscous region. The choice of the best fit followed the procedure described above: values of

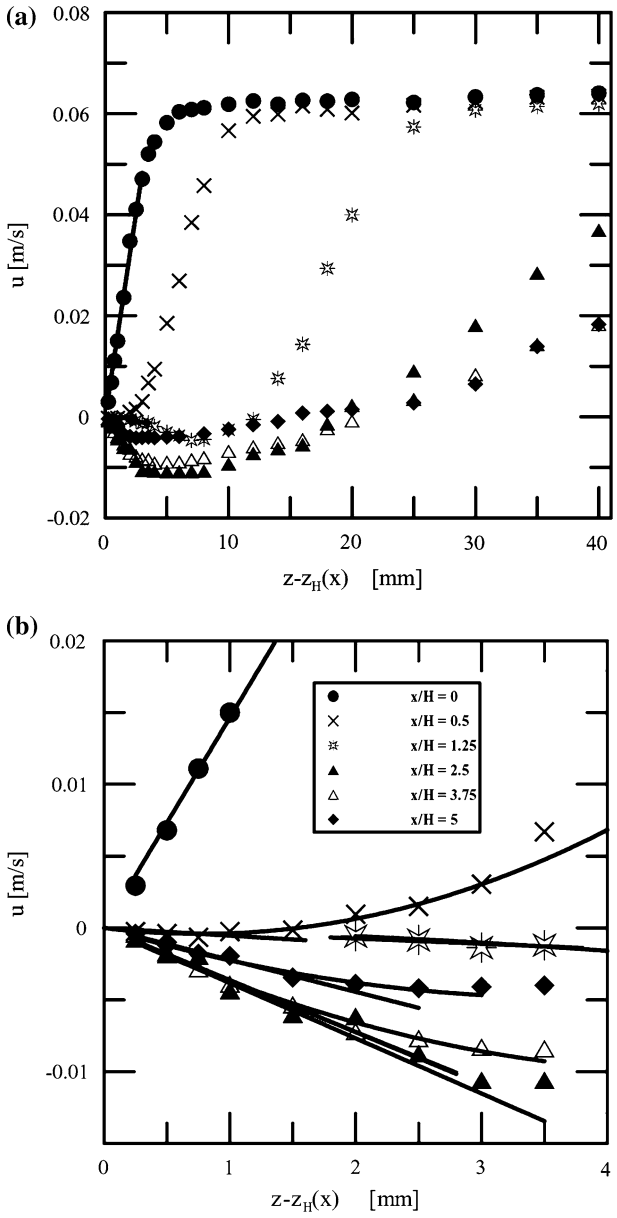

Fig. 10 **a** Mean velocity profiles at the hill top and in the reverse flow region. **b** Detail of the near wall behavior. Curve fits are shown as *solid lines*

R_{sq} that were closest to unity defined the best curve fits. Figure 10b shows, as solid lines, all 11 best fits that were found. Nine curves can be easily distinguished. The other two are difficult to spot for they coincide or are too close together ($x/H = 1.25$ and 2.5). The linear fit for the velocity profile on top of the hill stands out, showing how good a coefficient of correlation could be determined there ($R_{sq} = 0.998$). For the next station, $x/H = 0.5$, the linear fit was unable to capture the observed behavior. This is clearly illustrated in Fig. 10b, where a distinct non-linear behavior can be observed for the near wall velocity profile. A second degree polynomial fit applied to this station provided $R_{sq} = 0.981$ using eight points. At station $x/H = 1.25$, operational difficulties with the traversing gear system prevented us from getting data at distances smaller than 2 mm away from the wall and consequently, predictions of u_* from data fit were very poor. Nevertheless, we have decided to show the mean velocity data for $x/H = 1.25$ in Fig. 10b to illustrate how crucial it is to get data in the very near wall region. At stations $x/H = 2.5$ and 3.75, values of $\partial P/\partial x$ were nearly zero so that both the linear and the second degree polynomial fits provided very close results. The same observation holds for station $x/H = 5$ where fits with R_{sq} of 0.99 were obtained.

From the best linear fits to the velocity profiles in the viscous region, u_* was calculated straightforwardly by $u_* = \sqrt{\nu\gamma}$, where $\gamma = \partial u/\partial z$.

Tables 4, 5 and 6 show the resulting values of u_* and the corresponding R_{sq} found by the best-fits. These tables also show results obtained through other fitting procedures, which will be discussed next.

4.2 Logarithmic region analysis

Figure 11 presents the mean velocity profiles for stations $x/H = -12.5$, -5 and -2.5 in log-linear coordinates. Typically, the turbulent logarithmic region was characterized by eleven points in the interval $20 \leq z^+ \leq 140$. The classical logarithmic law of the wall region can be well-identified; solid lines represent the best curve fits. To find u_* from the log-law assumption, a previous knowledge of $\varkappa$ is required. Here, we have followed Coles (1956) and used $\varkappa = 0.4$.

Mean velocity profiles in log-linear coordinates for the hill top and the reverse flow region are shown in Fig. 12a. No definitive logarithmic sublayer, as predicted by the classical law of the wall, can be identified.

Other authors, e.g. Thompson and Whitelaw (1985), Simpson et al. (1981), remarked that in the separated flow region there seems to exist a logarithmic variation in the mean velocity profiles. However, values of the

Table 4 Values of u_* upstream of hill top

(x/H)	Type of fit	Points	R_{sq}	u_* (m/s)
–12.5	LTO	7	0.993	0.00276
–12.5	Log	11	0.993	0.00284
–5	LTO	7	0.999	0.00243
–5	Log	11	0.995	0.00305
–2.5	LTO	7	0.991	0.00317
–2.5	2DP	13	0.996	0.00363
–2.5	Log	12	0.990	0.00244
(x/H)	Type of fit	Points	σ	u_* (m/s)
–12.5	RS	5	0.00016	0.00242
–5	RS	5	0.00011	0.00208
–2.5	RS	5	0.00016	0.00214

LTO linear fit through origin, *2DP* second degree polynomial fit (Eq. 3), *Log* logarithmic fit (Eq. 6), *RS* Reynolds stress fit (Eq. 7), σ standard deviation for the mean Reynolds stress average

Table 5 Values of u_* in the reverse flow region

(x/H)	Type of fit	Points	R_{sq}	u_* (m/s)
0	LTO	8	0.998	0.00403
0.5	LTO	4	0.754	–0.000734
0.5	2DP	8	0.981	–0.00104
1.25	LTO	4	0.974	–0.00061
1.25	2DP	8	0.976	–0.00052
2.5	LTO	5	0.979	–0.00197
2.5	2DP	8	0.971	–0.00190
3.75	LTO	6	0.997	–0.00191
3.75	2DP	6	0.988	–0.00192
5	LTO	5	0.993	–0.00150
5	2DP	7	0.978	–0.00162

LTO linear fit through origin, *2DP* second degree polynomial fit (Eq. 3)

Table 6 Values of u_* downstream of the separated flow region

(x/H)	Type of fit	Points	R_{sq}	u_* (m/s)
6.67	LTO	5	0.982	0.00132
6.67	Log	13	0.967	0.00184
10	LTO	7	0.996	0.00238
10	Log	13	0.994	0.00204
15	LTO	5	0.995	0.00254
15	Log	13	0.959	0.00228
20	LTO	8	0.996	0.00263
20	Log	11	0.994	0.00200
(x/H)	Type of fit	Points	σ	u_* (m/s)
6.67	RS	5	0.00024	0.00226
10	RS	5	0.0008	0.00225
15	RS	6	0.00021	0.00241
20	RS	7	0.0004	0.00211

LTO linear fit through origin, *2DP* second degree polynomial fit (Eq. 3), *Log* logarithmic fit (Eq. 6), *RS* Reynolds stress fit (Eq. 7), σ standard deviation for the mean Reynolds stress average

wall shear stress evaluated from procedures based on the standard law of the wall yielded results in an order of magnitude smaller than those obtained through other techniques. Curve fits in regions of the flow where the mean velocity profiles appear to follow a logarithmic behavior are shown in Fig. 12a. A detailed view of the curve fits, shown in solid lines, is presented in Fig. 12b. The statistics pertaining to the fitted straight lines reveal a very poor fitting quality: $x/H = 0.5$, $R_{sq} = 0.024$; $x/H = 2.5$, $R_{sq} = 0.687$; $x/H = 5.0$, $R_{sq} = 0.190$. To obtain these curves, five to six points were considered in the range of $0.2 \leq z^+ \leq 3.0$. This is, in fact, approximately the same range used to find the slope of the mean velocity profile in the viscous sublayer. The outer region of profiles shown in Fig. 12a, on the other hand, are characteristic of inertial sublayers governed by the defect law (Coles 1956). Therefore, we are led to conclude that a logarithmic behavior of the flow in the separated flow region is a poor representation.

The mean velocity profiles for stations located downstream of the reverse flow region are shown in Fig. 13 in log-linear coordinates. Solid lines represent the best curve fits. The existence of well-defined logarithmic regions for all four profiles is evident. Some scatter was observed for the logarithmic velocity profile at $x/H = 15$, that resulted in a coefficient of correlation of 0.959. For the additional stations, coefficients of determination, R-squared, were higher than 0.99. The logarithmic profiles used basically thirteen points for their characterization in the interval $20 \leq z^+ \leq 150$.

4.3 Reynolds shear stress profile

To estimate u_* from Eq. 7 an average was taken from the square root measured values of $-\overline{u'w'}$ in the near wall region.

In fact, due to difficulties that were intrinsic to the measurement technique and to the geometrical arrangements of the instrumentation, Reynolds shear stress data could not be obtained as close to the wall as we felt it would be necessary. Typically, only distances above 7 mm were investigated. In fact, in undisturbed flow regions, the fully logarithmic region was normally located between 7 mm ($z^+ \geq 20$) and 20 mm ($z^+ \geq 55$) away from the wall. In this interval, by considering the Reynolds shear stress to be constant, consistent predictions were found.

In the separated flow region, no constant behavior of $-\overline{u'w'}$ was observed (see Fig. 9b). Consequently, u_* could not be estimated from $-\overline{u'w'}$ profiles along the recirculation region.

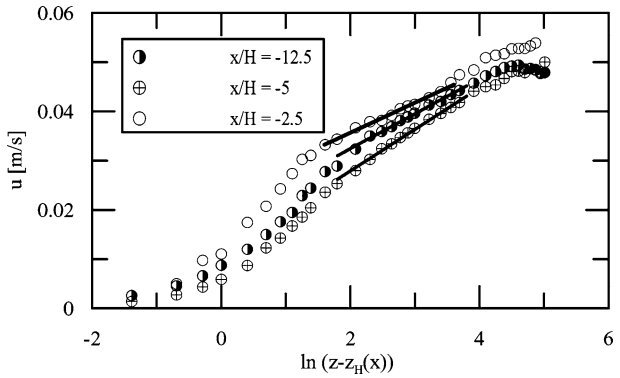

Fig. 11 Velocity profiles upstream of hill top. Please note the shift in origin according to Eq. 1

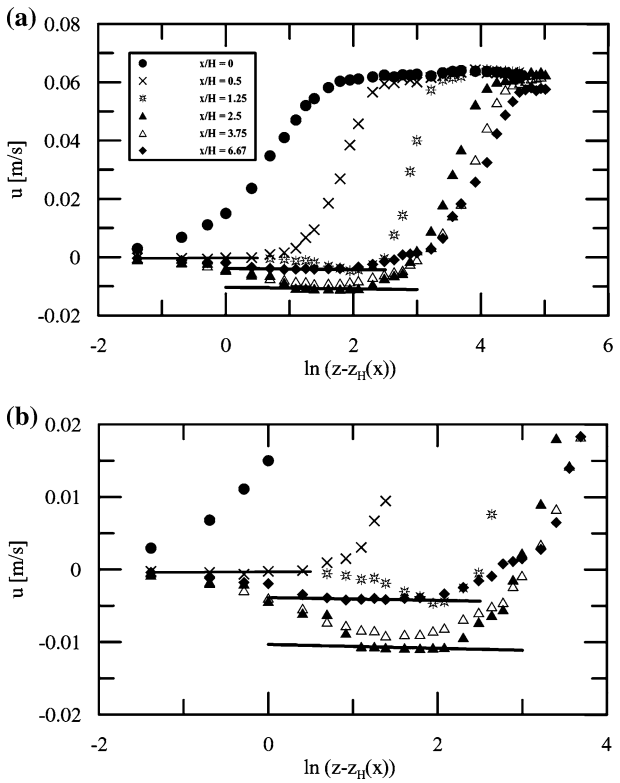

Fig. 12 **a** Velocity profiles in log-linear coordinates in the separated flow region, **b** details of the curve fits shown as *solid lines*

4.4 Wall shear stress consolidated results

Tables 4, 5 and 6 show that in general the linear fits provide the best R-squared values. The linear fit can then be regarded as the method that best represents the near wall data, thus providing the most accurate friction velocity results. Some scatter between the results was observed for the accelerated flow in the upwind slope of the hill when a difference of 35% was found between the four methods. However, for station

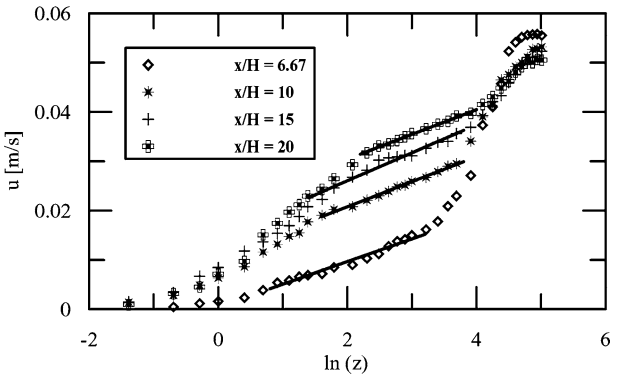

Fig. 13 Velocity profiles downstream of hill

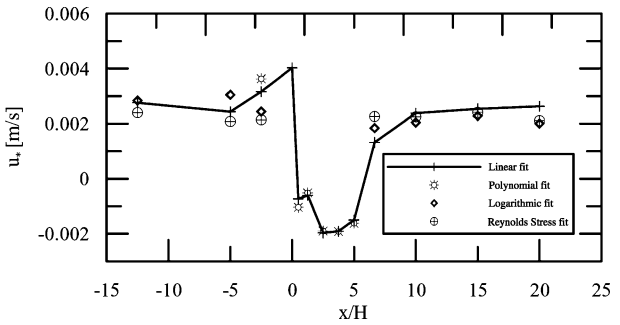

Fig. 14 Global behavior of friction velocity

$x/H = -2.5$, the agreement between the two values of u_* estimated from the linear and the polynomial fits is fairly good.

For the upstream undisturbed flow and the downstream reattached flow, the results obtained with all three methods agree reasonably well. In the reverse flow region, the two methods used to calculate u_*, the linear fit through origin and the polynomial fit, provided consistent results, particularly, at station $x/H = 3.75$.

Figure 14 consolidates the friction velocity results, considering all four methods that were used here.

5 Further turbulence results

Turbulence models that rely on the eddy viscosity concept are still widely used for they offer a good compromise between numerical effort and computational accuracy. This is a simple example of how the estimation of some flow properties such as the general form of the flow recirculation region, the mixing length and eddy viscosity profiles and the production terms might be of some interest. Provided one can accept that normal derivatives can be evaluated as a good approximate value from the measured rectangular

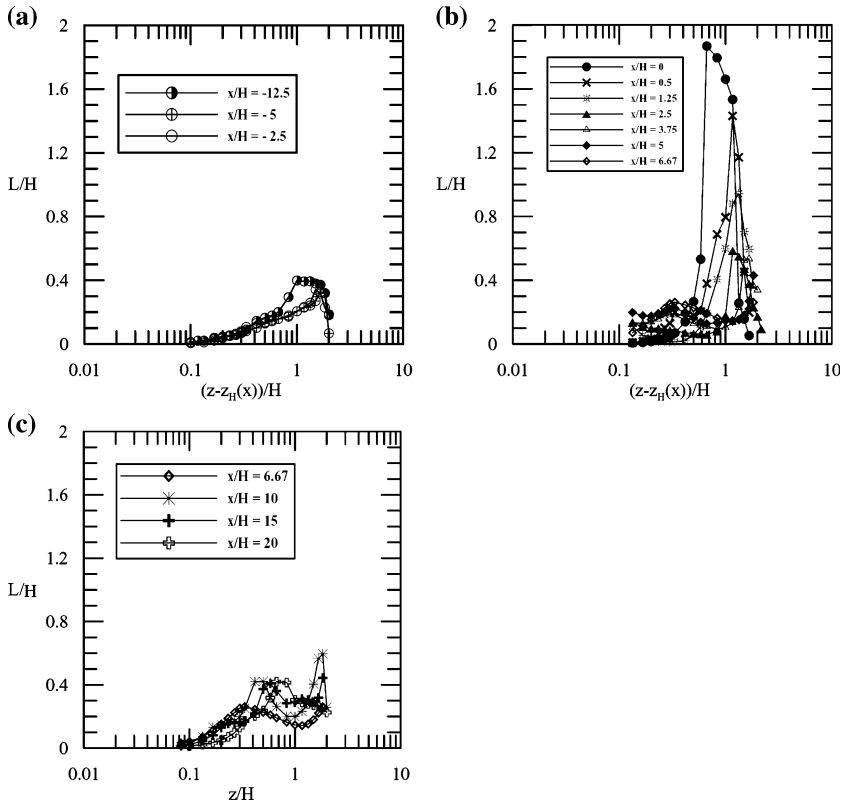

Fig. 15 Normalized mixing-length distribution, L/H: **a** upstream of the separation, **b** separation region, **c** downstream of the reattachment point

Cartesian profiles, at least an approximate behavior of these flow properties can be obtained.

The mixing-length and eddy viscosity distributions can be evaluated directly from the measured flow properties according to

$$\frac{L}{H} = \frac{(-\overline{u'w'})^{1/2}}{H}\left|\frac{\partial u}{\partial z}\right|^{-1}, \tag{9}$$

and

$$\frac{v_t}{u_\delta H} = \frac{-\overline{u'w'}}{u_\delta H(\partial u/\partial z)}, \tag{10}$$

where the mixing-length L is normalized by the hill height, H, and the eddy-viscosity distribution v_t is normalized by the undisturbed free-stream velocity, u_δ, and H.

Normalized mixing-length results are shown in Fig. 15 where solid lines are used to connect identical symbols. For stations x/H = –12.5, –5 and –2.5, Fig. 15a reveals that close to the wall all three mixing-length distributions collapse onto a single curve. In the outer region, however, the mixing-length experiences a continuous decrease as the fluid flows downstream. At the hill top, and at stations x/H = 0.5 and 1.25, L assumes very large values in the outer region due to the very little shear in the longitudinal velocity.

In the separated flow region, the mixing-length can only be defined at points where $\partial u/\partial z$ is positive. The general indication (Fig. 15b) is that L assumes relatively large values that are kept constant across the flow recirculation bubble. Downstream of the separation bubble, Fig. 15c, the mixing length tends to relax back to its standard behavior. In its return to equilibrium conditions, the inner layer mixing length distributions tend to collapse onto each other whereas the outer layer mixing length distributions do not experience a constant behavior as compared to undisturbed values. This corroborates that the inner region of the boundary layer returns to equilibrium faster than the outer sublayer, a characteristic noticed also by other authors in similar conditions, e. g., Song et al. (2000).

The eddy viscosity profiles are shown in Fig. 16. The behavior of v_t follows the general trends observed for L. The data indicate that uphill v_t decreases (Fig. 16a). At the top of the hill, and over the next two stations, the little shear in the outer region results in a large increase in v_t. The notable point, however, is that in the flow separated region v_t remains almost unchanged across x/H = 2.5. The large values of v_t close to the wall at stations x/H = 2.5, 3.75 and 5 are also a marked fact

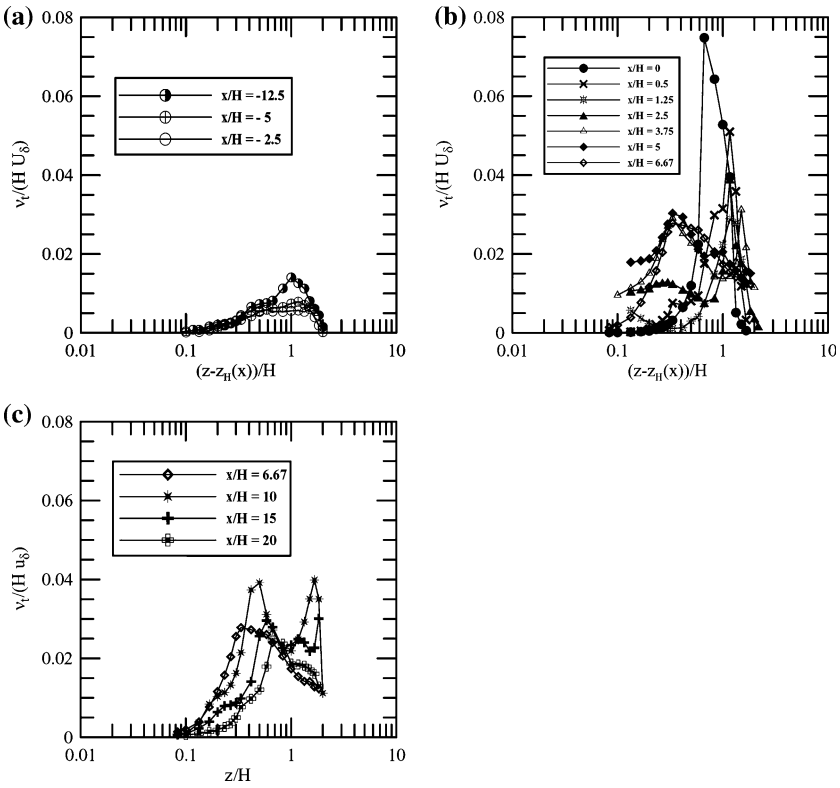

Fig. 16 Normalized eddy viscosity distribution, $v_t/(u_\delta\ H)$: **a** upstream of the separation, **b** separation region, **c** downstream of the reattachment point

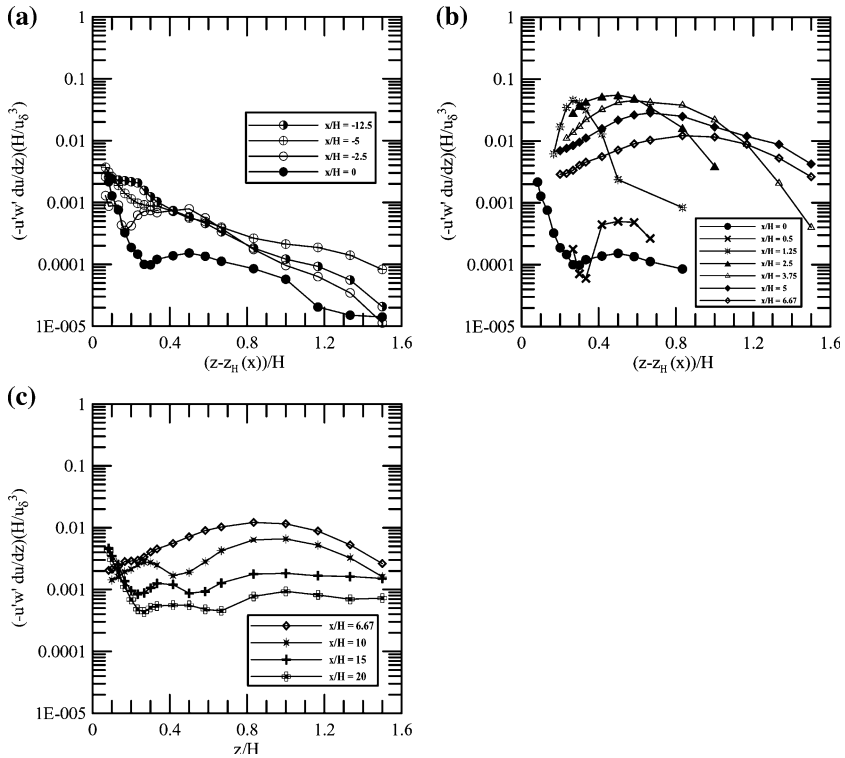

Fig. 17 Production term for the longitudinal Reynolds stresses, $P_{uu} = -\overline{u'w'}\mathrm{d}u/\mathrm{d}z$: **a** upstream of the separation, **b** separation region, **c** downstream of the reattachment point

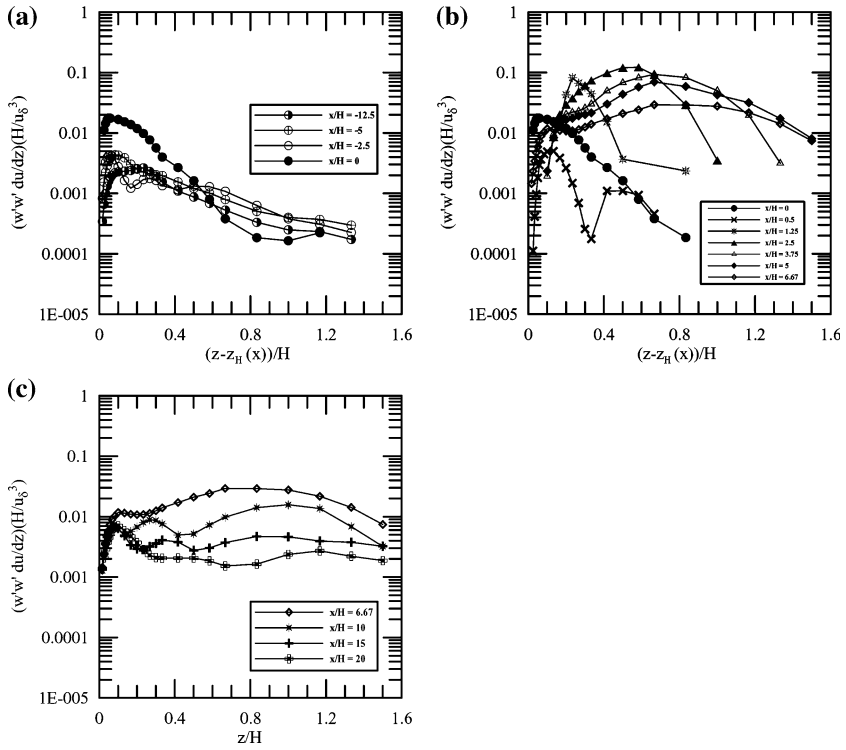

Fig. 18 Production term for the Reynolds shear stresses, $P_{-u'w'} = \overline{w'w'}\mathrm{d}u/\mathrm{d}z$: **a** upstream of the separation, **b** separation region, **c** downstream of the reattachment point

(Fig. 16b). The outer peaks observed in Fig. 16c, similar to the behavior of L, are due to changes in the outer region of the shear stresses and mean velocity profiles returning to equilibrium conditions.

The production terms in the transport equations for $\overline{u'^2}$ and $-\overline{u'w'}$ are shown in Figs. 17 and 18, respectively. These terms were normalized by the hill height, H and the free-stream undisturbed velocity u_δ; solid lines help to read the plots. For the upstream and downstream attached velocity profiles, the production terms $P_{uu} = -2\overline{u'w'}(\partial u/\partial z)$ and $P_{-uw} = 2\overline{w'w'}(\partial u/\partial z)$ reach a maximum very close to the wall. Approaching the top of the hill, P_{uu} decreases whereas P_{-uw} suffers a large increase. The production term P_{-uw} has an increase on top of the hill of about ten times its maximum upstream value. In fact, a difference of at least one order of magnitude is established between the two production terms at $x/H = 0$ (Figs. 17b, 18b). In the separated flow region, both production terms reach a maximum at station $x/H = 2.5$. The production term P_{uu} increases by at least one order of magnitude in the separated flow region as compared to its undisturbed upstream values. The same behavior is observed for P_{-uw} for it experiences a further ten-time increase in the separated flow region with the peak moving away from the wall.

6 Final remarks

We have carried out an experimental investigation of the flow around a steep smooth hill with the main purpose of providing good quality near-wall data to serve as a test-case for future analytical and numerical analyses of the problem. We hope the present results will be specially useful in scale analysis of the problem. The experimental data include mean velocity and turbulence profiles distributed over thirteen measuring stations. That distribution was shown to be detailed enough to provide a comprehensive flow description.

Four different methods were used to estimate the wall shear stress. The refined near-wall measurements allowed the friction velocity to be calculated through linear fits to mean longitudinal velocity profiles, as well as through polynomial fits in regions where pressure-gradients were important. In addition, curve fits to the logarithmic sublayer and to the region of constant Reynolds shear stress were used. The result was that the wall shear stress distribution for the whole flow field along the hill, in particular for the region of reverse flow, was presented. Results are shown to be consistent for the different u_* estimates.

Further results have also been presented, including the mixing length and eddy viscosity distributions, and the turbulence energy production terms.

Acknowledgments JBRL benefited from a Research Scholarship from the Brazilian Ministry of Education through CAPES. JBRL is also grateful to the Programme Alban, European Union Programme of High Level Scholarships for Latin America, identification number E03M23761BR, for the concession of further financial help regarding her stay at Oporto University. Authors are grateful to Prof. Maria Fernanda Proença and the staff of the Laboratory of Hydraulics of Oporto University for all their help in setting up the experimental facilities as well as for some useful discussions. We are also grateful to Mr. André Sampaio for his help with some of the measurements. APSF is grateful to the Brazilian National Research Council (CNPq) for the award of a Research Fellowship (Grant no 304919/2003-9). The work was financially supported by CNPq through Grant no 472215/2003-5 and by the Rio de Janeiro Research Foundation (FAPERJ) through Grants E-26/171.198/2003 and E-26/152.368/2002.

References

Afzal N (1983) Analysis of a turbulent boundary-layer subjected to a strong adverse pressure-gradient. Int J Eng Sci 21:563–576

Allen B, Brown AR (2002) Large-eddy simulation of turbulent separated flow over rough hills. Bound Layer Meteorol 102:177–198

Arya SPS, Capuano ME Fagen LC (1987) Some fluid modelling studies of flow and dispersion over two-dimensional low hills. Atmos Environ 21:753–764

Athanassiadou M, Castro IP (2001) Neutral flow over a series of rough hills: a laboratory experiment. Bound Layer Meteorol 101:1–30

Bevington PR (1969) Data reduction and error analysis for the physical sciences. McGraw-Hill, New York

Britter RE, Hunt JCR, Richards KJ (1981) Air flow over a two-dimensional hill: studies of velocity speedup, roughness effects and turbulence. Q J R Meteorol Soc 107:91–110

Castro IP, Apsley DD, (1997) Flow and dispersion over topography: a comparison between numerical and laboratory data for two-dimensional flows. Atmos Environ 31:839–850

Coles D (1956) The law of the wake in the turbulent boundary layer. J Fluid Mech 1:191–226

Cruz DOA, Silva Freire AP (1998) On single limits and the asymptotic behavior of separating turbulent boundary layers. Int J Heat Mass Transf 41:2097–2111

Cruz DOA, Silva Freire AP (2002) Note on a thermal law of the wall for separating and recirculating flows. Int J Heat Mass Transf 45:1459–1465

Dengel P, Fernholz HH (1990) An experimental investigation of an incompressible turbulent boundary layer in the vicinity of separation. J Fluid Mech 212:615–636

Durbin PA, Belcher SE (1992) Scaling of adverse-pressure-gradient turbulent boundary layers. J Fluid Mech 238:699–722

Durst F, Kikura H, Lekakis I, Jovanovic J, Ye Q (1996) Wall shear stress determination from near-wall mean velocity data in turbulent pipe and channel flows. Exp Fluids 20:417–428

Finnigan J J (1983) A streamlined coordinate system for distorted turbulent shear flows. J Fluid Mech 130:241–258

Gong W, Ibbetson A (1986) A wind-tunnel study of turbulent flows over model hills. Bound Layer Meteorol 49:113-148

Grant ALM (1992) The structure of turbulence in the near-neutral atmospheric boundary-layer. J Atmos Sci 49:226–239

Hewer FE (1998) Non-linear numerical model predictions of flow over an isolated hill of moderate slope. Bound Layer Meteorol 87:381–408

Hunt JCR, Leibovich S, Richards KJ (1988) Turbulent shear flows over a low hills. Q J R Meteorol Soc 114:1435–1471

Iizuka S, Kondo H (2004) Performance of various sub-grid scale models in large-eddy simulations of turbulent flow over complex terrain. Atmos Environ 38:7083–7091

Ishihara T, Fujino Y, Hibi K (2001) Wind tunnel study of separated flow over a two-dimensional ridge and a circular hill. J Wind Eng 89:573–576

Jackson PS, Hunt JCR (1975) Turbulent wind flow over a low hill. Q J R Meteorol Soc 101:929–955

Khurshudyan LH, Snyder WH, Nekrasov IV (1981) Flow and dispersion of pollutants over two-dimensional hills. Environment Protection Agency Report no EPA-600/4-81-067. Research Triangle Park, 130 pp

Logan SE (1972) A laser velocimeter for Reynolds stress and other turbulence measurements. AIAA J 10:933–935

Mason PJ, Sykes RI (1979) Flow over an isolated hill of moderate slope. Q J R Meteorol Soc 105:383–395

Mellor GL (1966) The effects of pressure-gradients on turbulent flow near a smooth wall. J Fluid Mech 24:255–274

Melnik RE (1989) An asymptotic theory of turbulent separation. Comput Fluids 17:165–184

Millikan CB (1939) A critical discussion of turbulent flow in channels and tubes. In: Proceedings of the 5th Int Cong App Mech J. Wiley, New York, pp 386–392

Nakayama A, Koyama H (1984) A wall law for turbulent boundary layers in adverse pressure-gradients. AIAA J 22:1386–1389

Naqwi AA, Reynolds WC (1987) Dual cylindrical wave laser—Doppler method for measurement of skin friction in fluid flow. Report TF-28, Stanford University

Prandtl L (1925) Über die ausgebildete Turbulenz. ZAMM 5:136–139

Ross AN, Arnold S, Vosper SB, Mobbs, SD, Dixon N, Robins AG (2004) Comparison of wind-tunnel experiments and numerical simulations of neutral and stratified flow over a hill. Bound Layer Meteorol 113:427–459

Simpson RL, Chew YT, Schivaprasad BG (1981) The structure of a separating boundary layer. Part 1: mean flow and Reynolds stresses. J Fluid Mech 113:23–51

Song S, DeGraaff D, Eaton JK (2000) Experimental study of a separating, reattaching, and redeveloping flow over a smoothly contoured ramp. Int J Heat Fluid Flow 21:512–519

Stratford BS (1959) The prediction of separation of the turbulent boundary layer. J Fluid Mech 5:1–16

Sychev VV, Sychev Vik V (1980) On turbulent separation. USSR Comput Maths Math Phys 20:133–145

Thompson BE, Whitelaw JH (1985) Characteristics of a trailing-edge flow with turbulent boundary layer separation. J Fluid Mech 18:1–57

Wang C, Jang YJ, Leschziner MA (2004) Modelling two- and three-dimensional separation from curved surfaces with anisotropy-resolving turbulence closures. Int J Heat Fluid Flow 25:499–512

Winter KG (1977) An outline of the techniques available for the measurement of skin friction in turbulent boundary layers. Prog Aero Sci 212:615–636

Ying R, Canuto VM (1997) Numerical simulation of the flow over two-dimensional hills using a second-order turbulence closure model. Bound Layer Meteorol 85:447–474